Chin. Geogra. Sci. 2012 Vol. 22 No. 1 pp. 63–74
doi: 10.1007/s11769-012-0514-4
www.springerlink.com/content/1002-0063

Estimating Fraction of Photosynthetically Active Radiation of Corn with Vegetation Indices and Neural Network from Hyperspectral Data

YANG Fei[1], ZHU Yunqiang[1], ZHANG Jiahua[2], YAO Zuofang[3]

(*1. The State Key Laboratory of Resources and Environmental Information System, Institute of Geographic Sciences and Natural Resources Research, Chinese Academy of Sciences, Beijing 100101, China; 2. The Laboratory of Remote Sensing and Climate Information, Chinese Academy of Meteorological Sciences, Beijing 100081, China; 3. The Beijing National Technology Transfer Center of Chinese Academy of Sciences, Beijing 100086*)

Abstract: The fraction of photosynthetically active radiation (FPAR) is a key variable in the assessment of vegetation productivity and land ecosystem carbon cycles. Based on ground-measured corn hyperspectral reflectance and FPAR data over Northeast China, the correlations between corn-canopy FPAR and hyperspectral reflectance were analyzed, and the FPAR estimation performances using vegetation index (VI) and neural network (NN) methods with different two-band-combination hyperspectral reflectance were investigated. The results indicated that the corn-canopy FPAR retained almost a constant value in an entire day. The negative correlations between FPAR and visible and shortwave infrared reflectance (SWIR) bands are stronger than the positive correlations between FPAR and near-infrared band reflectance (NIR). For the six VIs, the normalized difference vegetation index (NDVI) and simple ratio (SR) performed best for estimating corn FPAR (the maximum R^2 of 0.8849 and 0.8852, respectively). However, the NN method estimated results (the maximum R^2 is 0.9417) were obviously better than all of the VIs. For NN method, the two-band combinations showing the best corn FPAR estimation performances were from the NIR and visible bands; for VIs, however, they were from the SWIR and NIR bands. As for both the methods, the SWIR band performed exceptionally well for corn FPAR estimation. This may be attributable to the fact that the reflectance of the SWIR band were strongly controlled by leaf water content, which is a key component of corn photosynthesis and greatly affects the absorption of photosynthetically active radiation (APAR), and makes further impact on corn-canopy FPAR.

Keywords: hyperspectral remote sensing; corn; FPAR; vegetation index; neural network

Citation: Yang Fei, Zhu Yunqiang, Zhang Jiahua, Yao Zuofang, 2012. Estimating fraction of photosynthetically active radiation of corn with vegetation indices and neural network from hyperspectral data. *Chinese Geographical Science*, 22(1): 63–74. doi: 10.1007/s11769-012-0514-4

1 Introduction

The fraction of photosynthetically active radiation (FPAR) measures the proportion of photosynthetically available radiation that is absorbed by canopies in the specific spectrum of 400–700 nm. It is an important detection index for vegetation water, energy, and carbon balance and is a key parameter in many models, such as ecosystem productivity models and crop yield models (Sellers *et al.*, 1997; Lobell *et al*., 2003; FAO, 2007).

Remote sensing has become one of the most important methods for monitoring precision agriculture, the environment, and the ecosystem; it is a key tool for quantitatively estimating vegetation biophysical or biochemistry parameters, such as the leaf area index (LAI), chlorophyll, and FPAR (Chen and Cihlar, 1996; Myneni *et al.*, 2002). In recent years, hyperspectral remote sensing data have been widely used in the estimation of vegetation biophysical and biochemical parameters, as well as for object identification or classification (Lee *et al.*, 1999; Tian *et al.*, 2001; Melgani and Bruzzone, 2004; Yang *et al.*, 2010). Hyperspectral remote sensing reflec-

Received date: 2011-02-18; accepted date: 2011-04-08

Foundation item: Under the auspices of National Key Research Program of Global Change Research (No. 2010CB951302), National Natural Science Fundation of China (No. 40771146), China Postdoctoral Science Foundation Funded Project (No. 07Z7601MZ1)

Corresponding author: ZHANG Jiahua. E-mail: zhangjh@cams.cma.gov.cn

© Science Press, Northeast Institute of Geography and Agroecology, CAS and Springer-Verlag Berlin Heidelberg 2012

tance is the preferred tool for estimating FPAR because of its accurate depiction of the effect of leaf components on FPAR. Several hyperspectral sensors, such as the Earth Observing-1 Hyperion and the Airborne Visible Infrared Spectrometer, have been widely used in a broad range of applications. However, the major problem with hyperspectral remote sensing data is the proper use of the high dimensionality function to achieve a high level of accuracy during investigations and applications (Pu and Gong, 2004). Although the visible and near-infrared bands, from 4.0 μm to 1.0 μm, have been widely used, data on the shortwave infrared band (1.0–2.5 μm) have not been effectively applied in vegetation parameter estimation (Gong *et al*., 2003), such as FPAR.

At present, FPAR estimation mainly uses physical transfer models or empirical vegetation index (VI) methods, such as the normalized difference vegetation index (NDVI) and other indices with broadband spectral reflectance (Daughtry *et al*., 1992; Epiphanio, 1995). Ridao and Conde (1998) compared nine VIs to estimate the FPAR of corn and soybean crops based on measured data and studied the effect of the shortwave infrared reflectance (SWIR) band in Landsat TM5 and solar angles on the relationships between VIs and FPAR. LAI was also usually used for FPAR estimation, as vegetation canopy photosynthesis depends on the vegetation leaf area (Daughtry *et al*., 1992; Turner *et al*., 2002). In addition, a few simple or complicated physical transfer models (McCallum *et al.*, 2010), such as the scattering by arbitrarily inclined leaves (Goward and Huemmrich, 1992; Huemmrich and Goward, 1997), the three-dimensional physical transfer model (Knyazikhin *et al*., 1998a; 1998b; Myneni *et al*., 2002), and the analyses of interaction process between photons and canopy (Tao *et al.*, 2009) have been used to simulate FPAR. However, in terms of the complex defect, the physical model has not been widely used for high temporal and spatial FPAR estimation.

The neural network (NN) method has increasingly been used in interpreting remotely sensed data because of its high computational efficiency and accurate approximation of complex nonlinear functions (Krasnopolsky and Chevallier, 2003). Its data-analyzing procedure, which is based on the ′black box′ approach, can overcome the effects of any subjective activities. Recently, the NN method has also been widely used in biophysical parameters estimation (e.g., LAI) (Smith, 1993; Fang *et al.*, 2003; Walthall *et al.*, 2004; Bacour *et al.*, 2006). The NN method has been proved to be an ideal method for extracting information from multi- or hyper-dimensional data. However, it has scarcely been used for FPAR estimation, especially in extracting hyperspectral information to estimate crop canopy FPAR.

Hyperspectral reflectance shows much more abundant spectral information than methods that commonly used broad bands do. The empirical methods of VI and NN are also often used for vegetation parameter estimation because of their efficient computation and high estimation accuracy capabilities. The main objectives of this study are to investigate the corn FPAR estimation using hyperspectral reflectance, VI and NN, to identify the key bands or their combinations that could potentially improve corn FPAR estimation performance, and also to evaluate the VI and NN methods for crop canopy FPAR estimation performance in Jilin Province, China.

2 Materials and Methods

2.1 Study area

The study area (43°47′–44°53′N, 125°15′–126°24′E) is located in the suburb of Changchun proper and field farmland of Dehui City of Jilin Province in Northeast China (Fig. 1). The elevation ranges from 155 m to 200 m. Corn is the dominant crop in the study area with a planted area of 302 024 ha, which accounts for 76.65% of the farmland area. The uppermost soil type in the study area is black soil (i.e., it is part of the world-famous black soil zone in Northeast China). The local climate is a semi-humid, monsoon climate; the mean annual temperature is 5.55℃; and the mean annual precipitation is 471.5 mm. The sunshine in this area is 2631 hours per year; the accumulated temperature is 2851℃ during crop growing period (from May to September); and the frost-free period is 142 days.

2.2 Data collection

The field measurement data were collected at the Changchun Experimental Station of Jilin Agricultural University on August 19, 2006 and on June 15, July 5 and July 22, 2007, respectively, and there was a one-time measurement from the corn field in Dehui City on August 6, 2007. Totally, 99 data samples were collected in this study. Because the corn growth stage in the study area is from the June to September, the LAI is

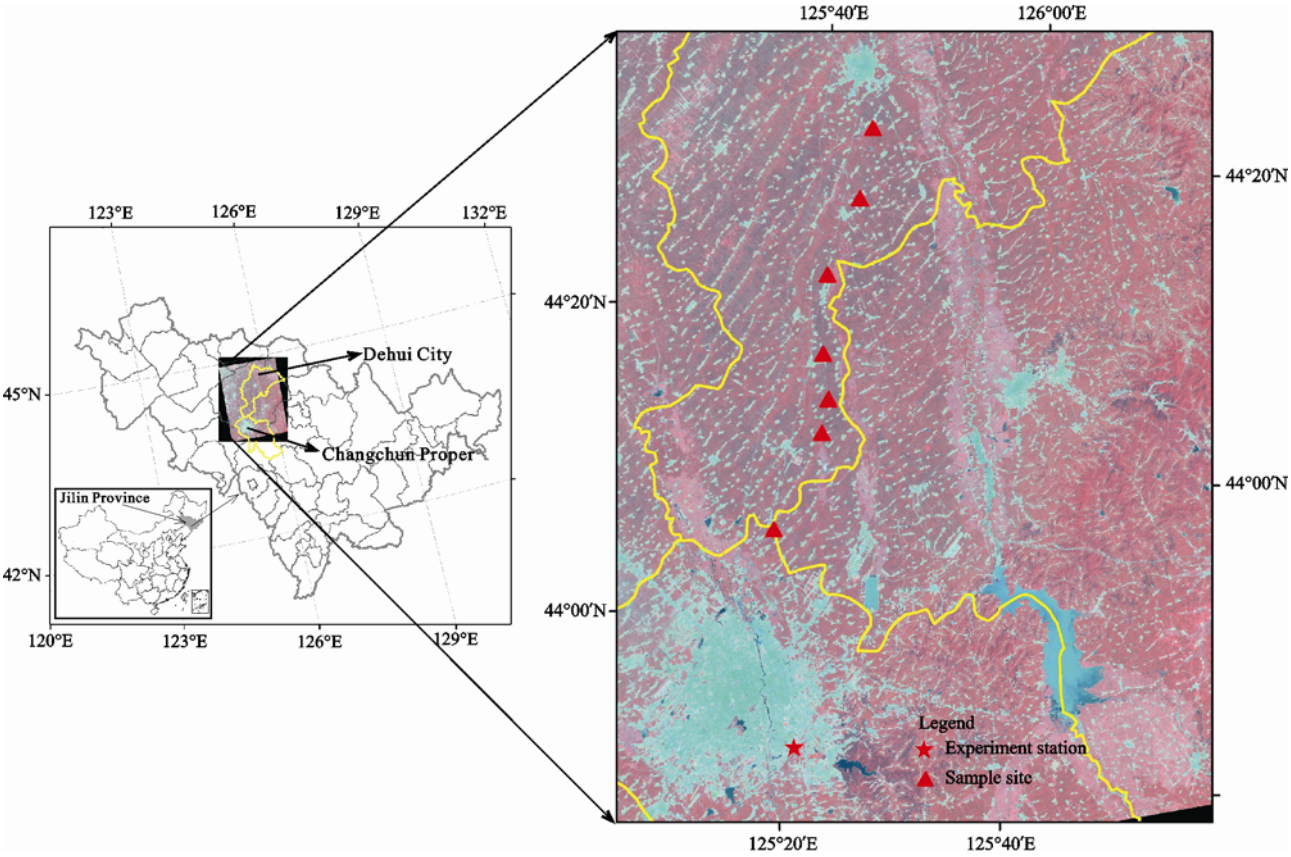

Fig. 1 Location of study area and distribution of sampling sites

very small (about 0.3 around) on June and arrived to the largest in the silking-tasseling period on August (Song, 2005), and that the measured data in the five periods of the corn growth could almost represent the corn canopy parameters changes in the whole growth period.

2.2.1 Field FPAR data acquisition

The FPAR was measured with a LI-191SA linear quantum sensor and a LI-250A light meter (LI-COR, Inc. USA). The LI-191SA inductive area was 1 m × 12.7 mm, and its inductive wavelength ranged from 400 nm to 700 nm, with a logging unit of μmol/(m^2·s). The logged data were identified as the average photosynthetically active radiation (PAR) in the inductive area which could reduce spatial heterogeneity effects. A LI-250A was used to log the results, and the data were manually read and written down. In each sampling site, four fractions of PAR data, including the incidence PAR above the canopy (PAR_{ci}), the transmitted PAR through the canopy (PAR_{gi}), and the reflected PAR by the canopy (PAR_{cr}) and the soil (PAR_{gr}), were measured. The FPAR was computed from these four fractions (Gallo and Daughtry, 1986; Widlowski, 2010):

$$FPAR = \frac{(PAR_{ci} - PAR_{cr}) - (PAR_{gi} - PAR_{gr})}{PAR_{ci}} \quad (1)$$

2.2.2 Hyperspectral reflectance acquisition

The spectro-radiometer of FieldSpec Pro FR made by Analytical Spectral Devices Corporation in USA, was used for measuring the corn canopy hyperspectral reflectance. Its field of view is 25°, its spectral range is 350–2500 nm, the spectral resolutions of 350–1000 nm and 1000–2500 nm are 3 nm and 10 nm, respectively, and its re-sampling interval of reflectance is 1 nm. The fiber probe was kept vertically above the corn canopy at 1.5 m. When the corn crops were too high in the later growth stages, a ladder was used to help keeping the fiber vertical. In every sampling site, to reduce the effects of weather conditions, the spectro-radiometer was calibrated with a white board before collecting data.

2.3 Methods

2.3.1 Correlation analysis and vegetation index method

The correlation analysis was conducted to identify the relationships between the FPAR and the reflectance in

every band. The VI is important in vegetation studies when dealing with remote sensing data (Ridao and Conde, 1998; Gong *et al.*, 2003). In this investigation, six VIs (Table 1), belonging to three kinds of VIs: the normalized difference index, ratio index, and orthogonal index (Zhao, 2003), were used for the corn FPAR estimation. Different band combinations from hyperspectral reflectance data were analyzed.

2.3.2 Neural network method

The neural network (NN) is increasingly being used for vegetation parameters estimation, and its estimation performance essentially relies on the training database (distribution of inputs and outputs) and the training process (Bacour *et al.*, 2006). In general, the training processes are conducted to explore the intrinsic relationships of inputs and their corresponding outputs (Kimes *et al.*, 1998); the weighted coefficients of the input variables are adjusted iteratively under this condition. In this study, the NN relied on the minimization of a misfit function by a back-propagation algorithm that is comprised of three layers: one input layer with the trainlm function, exploited by Levenberg-Marquardt and characterized by efficient operation (i.e., fast convergence); one hidden layer with a tangsig transfer function; and one output layer with a purelin transfer function and one neuron (i.e., the estimated FPAR). The goal root mean square error of the network was set to 0.01, and the training iterative time was 1000. Two-band combinations were set as the input data for the NN, and the number of middle-layer elements was changed from 2 to 10. Sixty randomly selected data samples were used to train the network. Band combinations corresponding to the best regression result between the modeled FPAR and the measured FPAR were determined, and these were used to model the canopy FPAR of the other 39 samples.

2.4 Precision evaluation

In this study, the determination coefficients (R^2) and root mean square error (*RMSE*) were used to evaluate corn FPAR estimation performance, and they were computed separately by the following equations,

$$R^2 = \frac{[\sum_{i=1}^{n}(Y_{\text{mea}} - \overline{Y_{\text{mea}}})(Y_{\text{mod}} - \overline{Y_{\text{mod}}})]^2}{\sum_{i=1}^{n}(Y_{\text{mea}} - \overline{Y_{\text{mea}}})^2 (Y_{\text{mod}} - \overline{Y_{\text{mod}}})^2} \quad (2)$$

$$RMSE = \sqrt{\frac{\sum_{i=1}^{n}(Y_{\text{mod}} - Y_{\text{mea}})^2}{n-1}} \quad (3)$$

where Y_{mod} is the FPAR estimated by the estimation model, $\overline{Y_{\text{mod}}}$ is the mean of the estimated FPAR, Y_{mea} is the measured FPAR, $\overline{Y_{\text{mea}}}$ is the mean of measured FPAR, and n is the number of samples for validation. The two indices were used to explore the correlation between the modeled and measured FPAR. The higher the R^2 or the smaller the *RMSE* is, the more similar are the values of the modeled and measured FPAR.

3 Results and Analyses

3.1 Daily changes in corn canopy FPAR

To obtain reliable measured data, it is necessary to accurately understand the FPAR changes within an entire day. Figure 2 shows the daily changes in the corn FPAR on a sunny day on August 19, 2006 (i.e., corn filling period); these changes were based on the FPAR mean value of six groups from field measurement data. The

Table 1 Summary of two-band vegetation index analyzed in this study

Vegetation index	Formula	Reference
Normalized difference vegetation index (NDVI)	$NDVI = (\rho_{\text{NIR}} - \rho_{\text{R}}) / (\rho_{\text{NIR}} + \rho_{\text{R}})$	Rouse *et al.*, 1974
Simple ratio (SR)	$SR = \rho_{\text{NIR}} / \rho_{\text{R}}$	Jordan, 1969
Perpendicular vegetation index (PVI)	$PVI = (\rho_{\text{NIR}} - a \times \rho_{\text{R}} - b) / (1 + a^2)^{1/2}$	Lyon *et al.*, 1998
Renormalized difference vegetation index (RDVI)	$RDVI = (\rho_{\text{NIR}} - \rho_{\text{R}}) / (\rho_{\text{NIR}} + \rho_{\text{R}})^{1/2}$	Roujean and Breon, 1995
Soil adjusted vegetation index (SAVI)	$SAVI = (\rho_{\text{NIR}} - \rho_{\text{R}})(1 + L) / (\rho_{\text{NIR}} + \rho_{\text{R}} + L)$	Huete, 1988
Transformed soil adjusted vegetation index (TSAVI)	$TSAVI = [a(\rho_{\text{NIR}} - a \times \rho_{\text{R}} - b)] / (a \times \rho_{\text{NIR}} + \rho_{\text{R}} - ab)$	Baret *et al.*, 1989

Notes: ρ_{B}, ρ_{R}, ρ_{NIR} and ρ_{SWIR} are the reflectance of blue, red, near-infrared and shortwave bands; a and b are the slope and offset of the soil line, and they were calculated from the filed measured soil hyperspectral reflectance in the study area, a = 1.0578, b = 0.0688; L is the adjusting coefficients, L = 0.5

FPAR varied from 0.90 to 0.95 within a single day, and the mean FPAR was approximately 0.924 during the corn growth stage. The corn canopy FPAR was relatively stable in the morning (8:00 to 10:30 AM) and in the afternoon (13:00 to 16:00 PM), but the FPAR showed slight fluctuations from 10:30 AM to 13:00 PM, with a maximum FPAR bias of about 0.03. These fluctuations occurred because the solar elevation angle was too large and the sunshine was coming from above the canopy. As a result, the area irradiated by solar radiation was relatively small.

Therefore, to accurately acquire the FPAR data, the field FPAR measurements in this study were conducted in the morning or in the afternoon, when the corn canopy FPAR was relatively stable.

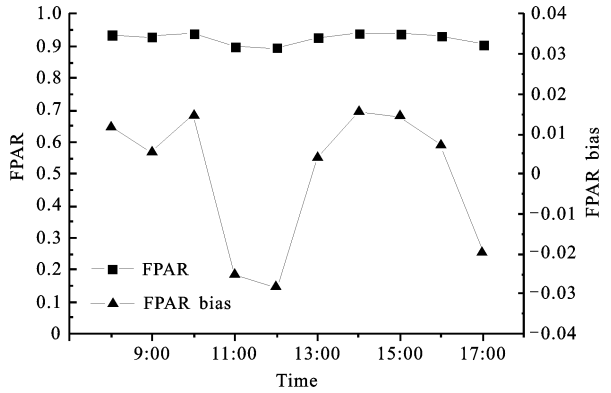

Fig. 2 Daily changes in corn FPAR and their bias

3.2 Correlations between corn FPAR and hyperspectral reflectance

The strong relationship between the corn FPAR and hyperspectral reflectance in most bands is shown in Fig. 3. The visible and SWIR band reflectance has negative correlations with the corn FPAR (i.e., maximum R of –0.871 and –0.888). However, positive correlations between the FPAR and the NIR band reflectance were obtained (i.e., maximum R of 0.778). In general, the PAR corresponds to the solar radiation at 400–700 nm in the visible band, so the corn FPAR behaved the inherent correlation with the visible band. The FPAR were determined by the vegetation canopy leaf area index, and the NIR bands are also very sensitive to the canopy leaf area, therefore, the FPAR also has good correlations with the NIR reflectance. The SWIR band reflectance is controlled mainly by the leaf water content, which plays an important role in vegetation photosynthesis and greatly affects vegetation absorption to PAR (Carter, 1991; Zarco-Tejada *et al.*, 2003), and this may be the reason why the FPAR is also highly correlated with the SWIR bands.

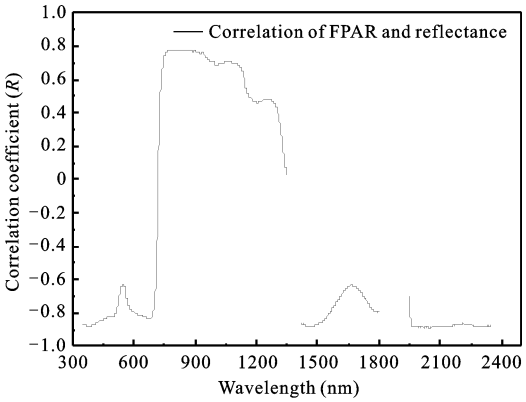

Fig. 3 Correlation of FPAR and reflectance (n = 99)

3.3 Corn FPAR estimation with VI from different band combinations

Several VIs were computed by using the combinations of different bands from visible to SWIR bands. The determination coefficients (R^2) of FPAR and the VIs with different band combinations were analyzed. To avoid any random fluctuation of the narrow band, the field measured hyperspectral reflectance was re-sampled referencing the Hyperion sensor channels by its central wavelength (CW) and the full width at half the maximum (FWHM). The bands of the field-measured hyperspectral reflectance at the ranges of 426.82–1341.2 nm, 1421.94–1800.29 nm and 1951.57–2395.5 nm were considered. Bands at the ranges of 1351.3–1411.89 nm and 1810.38–1940.57 nm were neglected because they were greatly affected by the atmospheric water vapor and consequently exhibited irregular fluctuations. In total, 175 bands were used for VI computation and correlation analysis with the FPAR. For each VI, an R^2 matrix was constructed from every two-band combination index (Fig. 4). Band 2 and band 1 were used in place of the NIR and visible bands for every VI, respectively. Based on the R^2 matrixes, the band combinations with high correlations for VI and FPAR were examined. In Fig. 4, the different color corresponds to the different R^2 grades, and the percentage of different R^2 value range is also presented with the pie chart. In Table 2, the band centers and ranges with good correlations to reflectance combinations with the FPAR are listed.

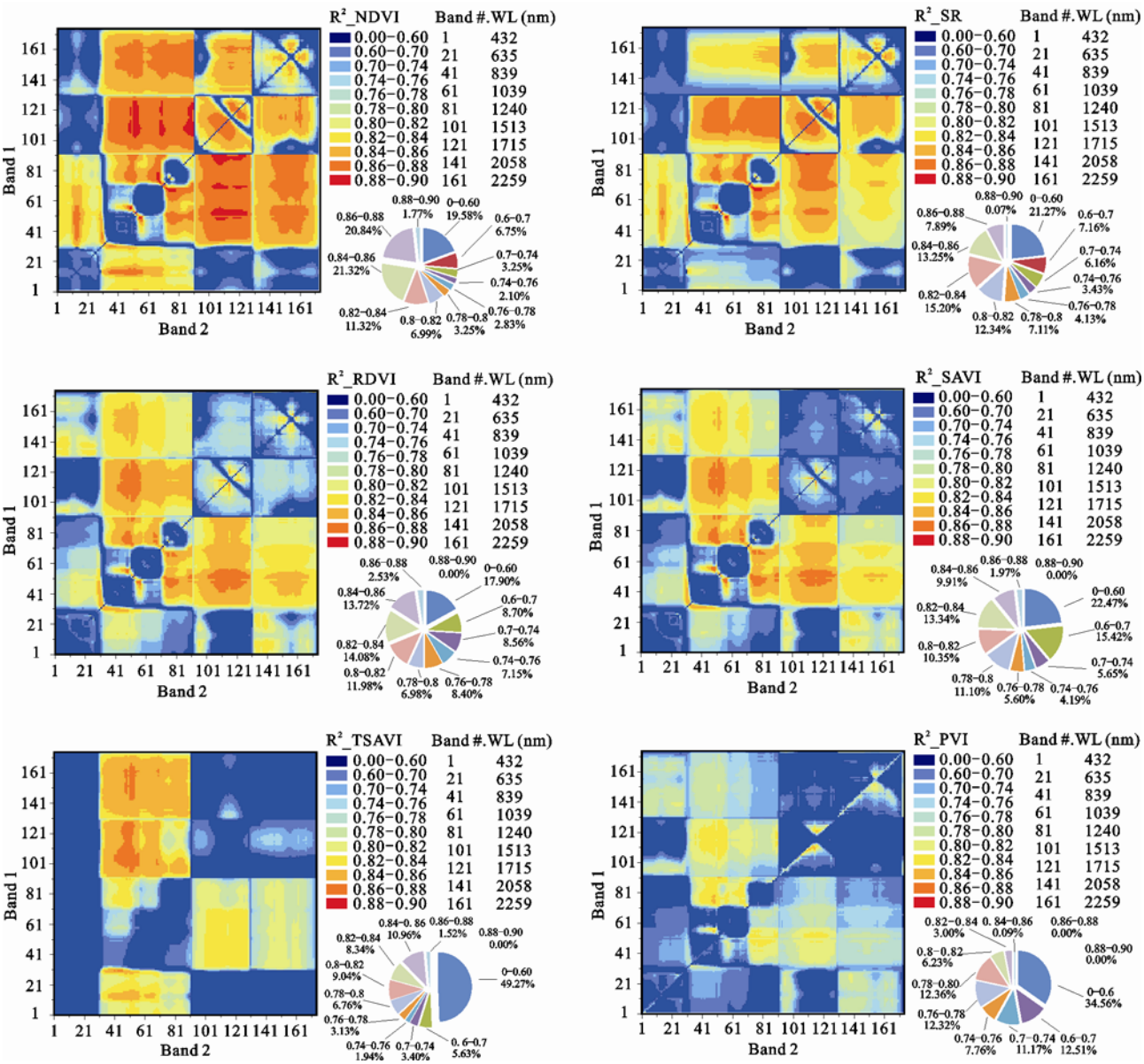

R^2 matrix plots show the correlations between the FPAR and vegetation indices that were computed from different band combinations among 175 bands spread across 430–2400 nm. Band 2 and band 1 are two variables of near-infrared input and visible input in the vegetation index; the wavelengths corresponding to the bands' numbers (Band #.) were marked

Fig. 4 R^2 matrix plots of the six vegetation indices

The results of Fig. 4 show that the R^2 matrix of the NDVI, RDVI and SAVI are symmetrical along the diagonal, whereas the others were not. Overall, the NDVI exhibited better correlations with the FPAR as compared to the other vegetation indices, which indicated larger R^2 from more band combinations. The maximum R^2 of the NDVI and SR matrices were both 0.885. In addition, 1.77% and 0.07% of the band combinations for NDVI and SR showed significant correlations with FPAR, the R^2 are all larger than 0.88. But no band combinations showing R^2 larger 0.88 were observed from the other four VIs. The R^2 matrixes of RDVI, SAVI and TSAVI exhibited moderate correlations with corn FPAR, their maximum R^2 were 0.872, 0.872 and 0.868, respectively. Moreover, in comparison of R^2 ranging from 0.86 to 0.88, the band combinations accounted for 2.53%, 1.97% and 1.52% separately for RDVI, SAVI and TSAVI. But they were still a little lower than those for NDVI and SR accounting for 20.84% and 7.89%. In addition, the PVI exhibited a lowest R^2 with FPAR (the

Table 2 Potential hyperspectral bands for six vegetation indices applied for corn FPAR estimation

VI	R^2	Band number in VI	Band center (nm)	Band range (nm)	Band description (spectral region and possible absorption features)
NDVI	≥ 0.87	1	1094	50	NIR-SWIR region, lignin and oil absorption
		2	1200	40	SWIR region, water, cellulose, starch, lignin absorption
		1	915	170	NIR region, protein and oil absorption
		2	1200	280	SWIR region, water**,** cellulose, starch, lignin absorption
		1	915	170	NIR region, protein and oil absorption
		2	1643	242	SWIR region, protein, nitrogen, lignin, cellulose, sugar and starch absorption
SR	≥ 0.87	1	1099	40	NIR-SWIR region, lignin and oil absorption
		2	1200	60	SWIR region, water, cellulose, starch and lignin absorption
		1	1321	40	SWIR region, water absorption
		2	1659	150	SWIR region, lignin, cellulose, sugar, starch and protein absorption
		1	1593	40	SWIR region, starch and sugar absorption
		2	1643	40	SWIR region, protein, nitrogen, lignin, cellulose, sugar and starch absorption
RDVI	≥ 0.86	1	915	10	NIR region, protein and oil absorption
		2	988	20	NIR region, starch absorption
		1	915	20	NIR region, protein and oil absorption
		2	1205	70	SWIR region, water, cellulose, starch and lignin absorption
		1	933	110	NIR region, oil absorption
		2	1653	160	SWIR region, protein, nitrogen, lignin, cellulose, sugar and starch absorption
PVI	≥ 0.82	1	1674	140	SWIR region, lignin and starch absorption
		2	910	180	NIR region, protein and oil absorption
		1	1255	170	SWIR region, water, cellulose, starch and lignin absorption
		2	889	80	NIR region, protein absorption
		1	920	40	NIR region, protein and oil absorption
		2	1230	140	SWIR region, water, lignin, cellulose and starch absorption
		1	947	20	NIR region, oil and water absorption
		2	1669	150	SWIR region, lignin and starch absorption
		1	1240	130	SWIR region, water, lignin, cellulose and starch absorption
		2	1099	30	NIR region, lignin and oil absorption
SAVI	≥ 0.86	1	967	300	NIR region, water and starch absorption
		2	1255	170	SWIR region, water, cellulose, starch, lignin absorption
		1	933	90	NIR region, oil absorption
		2	1669	140	SWIR region, lignin and starch absorption
		1	1099	20	NIR region, lignin and oil absorption
		2	1200	40	SWIR region, water, cellulose, starch, lignin absorption
TSAVI	≥ 0.86	1	1643	300	SWIR region, protein, nitrogen, lignin, cellulose, sugar, starch absorption
		2	929	60	NIR region, oil absorption
		1	2198	220	SWIR region, protein and nitrogen absorption
		2	952	40	NIR region, oil and water absorption

Notes: R^2 represents the optimal correlation. The boldface chemicals are principal for the absorption features (Curran, 1989; Gong *et al*., 2003). VI, vegetation index; NDVI, normalized difference vegetation index; SR, simple ratio; RDVI, renormalized difference vegetation index; PVI, perpendicular vegetation index; SAVI, soil adjusted vegetation index; TSAVI, transformed soil adjusted vegetation index; NIR, near infrared; SWIR, shortwave infrared

maximum R^2 of 0.852), and only 3.09% of the band combination showed a correlation with R^2 ranging from 0.82 to 0.86.

As for all of the VIs, as shown in Tables 2 and Table 3, all of the important band combinations presenting strong correlation between the VIs and the corn FPAR are within the NIR and SWIR regions. The results of Table 3 indicates that the VI computed from the SWIR

Table 3 Comparison of band combinations for estimating FPAR by vegetation index between optimal R^2

VI	FPAR estimated by SWIR and NIR band			FPAR estimated by V and NIR band		
	Optimal R^2	Wavelength (nm) band 1	Wavelength (nm) band 2	R^2	Wavelength (nm) band 1	Wavelength (nm) band 2
NDVI	0.885	1331.1	1593.5	0.820	645.0	860.0
SR	0.885	1109.2	1179.8	0.725	645.0	860.0
RDVI	0.872	988.1	910.1	0.803	645.0	860.0
PVI	0.852	1623.8	1654.0	0.715	645.0	860.0
SAVI	0.872	988.1	910.1	0.788	645.0	860.0
TSAVI	0.868	937.7	1563.2	0.818	645.0	860.0

and NIR bands obtained better correlations with FPAR than the VI usually calculated from the visible and NIR bands did. The optimal R^2 values were all above 0.852 for FPAR with the VIs computed from the SWIR and NIR bands. But the FPAR estimation of the R^2 by the VI calculated from visible and NIR bands ranged from 0.715 to 0.820.

The SWIR band showed great potential and acceptable performance for FPAR estimation, and this could be attributed to the SWIR band reflectance that were dominated mainly by the leaf water content (Table 2). Meanwhile, the leaf water plays an important role in vegetation photosynthesis and affects vegetation absorption in relation to PAR. The NIR and SWIR band reflectance with long wavelength functioned as the key feedback indicator of canopy FPAR (Curran, 1989; Carter, 1991; Gong *et al.*, 2003; Zarco-Tejada *et al.*, 2003).

As for the six VIs, only the PVI, SAVI and TSAVI obtained a little worse correlation with the FPAR, as compared to NDVI, SR and RDVI. This finding indicates that even if the field measurements were collected during the whole crop growth period, with the LAI varying from 0.1 to 4.4, the soil line-adjusted VI could not improve the correlations with the FPAR in this investigation, the soil offered little effect on the correlations between the VI and FPAR.

3.4 Corn FPAR estimation with NN

This study also investigated corn FPAR estimation performance with an NN method that was trained by different two-band combinations from visible to SWIR band reflectance. The R^2 and *RMSE* between the measured FPAR and estimated FPAR by the NN method were also determined. In Fig. 5, the matrix plots showed that the two-band combinations trained the NN well and exhibited much acceptable FPAR estimation performances. In particular, 47.92% of the R^2 values were higher than 0.88, and 51.96% of the *RMSE* values were between 0.10 and 0.12. Furthermore, the R^2 values of the measured and estimated FPARs, with combinations of visible bands at 523–584 nm and near-infrared bands at 757–1129 nm, were higher than 0.90. The *RMSE* values were lower than 0.10.

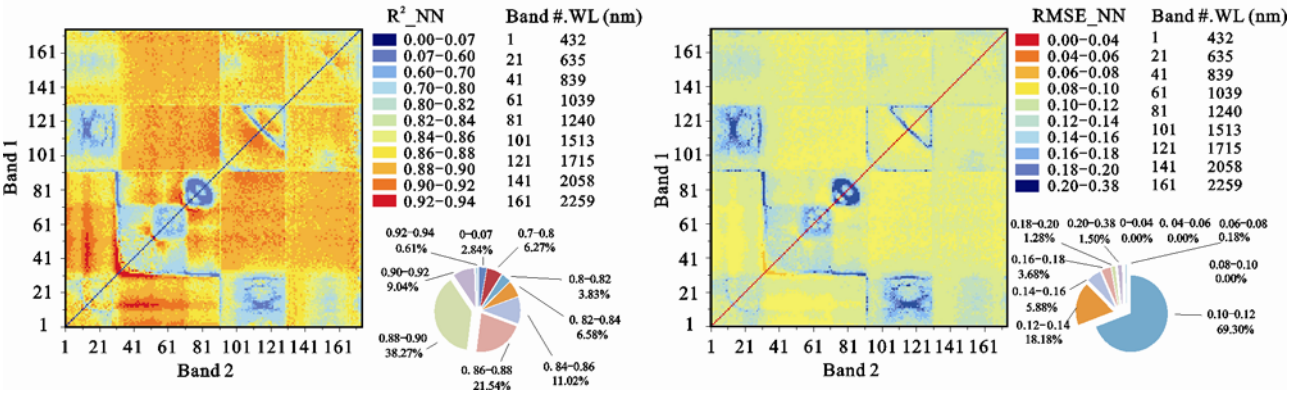

R^2 and *RMSE* matrix plots show the correlations between the measured FPAR and the NN-estimated FPAR by different two-band combinations
The figures description can be referred from Fig. 4

Fig. 5 R^2 and *RMSE* matrix plots for FPAR estimation by NN method

3.5 Comparison of VI and NN for corn FPAR estimation performances

Table 4 showed the band combinations percentage of the different R^2 ranges for corn FPAR estimation by these methods. By referring to different two band combinations, a comparison of Fig. 4, Fig. 5 and Table 4 revealed that the NN exhibited obviously a better estimating performance for corn FPAR than the Vis did. The maximum R^2 for estimating corn FPAR by NN method is 0.9417. For NDVI, the maximum R^2 was 0.8849, whereas the maximum R^2 values for other VIs were much lower. In addition, 9.6% of the band combinations using the NN method obtained an R^2 higher than 0.90, and 69.05% of the band combinations presented R^2 higher than 0.86. The R^2 values higher than 0.86 were 22.61% for the NDVI, 7.95% for the SR, 2.53% for the RDVI, 1.97% for the SAVI, and 1.52% for the TSAVI, respectively. The R^2 values between the PVI and the FPAR were all below 0.86.

4 Discussion

In this investigation, the six VIs could be classified into three types of structure indices: the normalized index, ratio index, and orthogonal index (Zhao, 2003). The results from this study showed that the normalized indices (including the NDVI, SAVI, and RDVI) exhibited the best FPAR performance, followed by the ratio indices of the SR and TSAVI, while the orthogonal index of PVI performed worst.

For these VIs, most of the band combinations from the SWIR and NIR bands displayed the best FPAR estimation performances, but for the NN, most of the band combinations from the NIR and the visible bands displayed the best FPAR estimation performances. And meanwhile, the reflectance in SWIR and NIR bands fluctuate greatly for different corn cover fraction, which could be much sensitive to the canopy parameters variation. But as NN, it was determined greatly based on the difference between real data and modeled data, to adjust iteratively the weighted coefficients of the input variables (Bacour *et al.*, 2006), so the NN method often gets better performance than Vis does on parameter estimation, such as LAI, chlorophyll (Fang *et al.*, 2003; Walthall *et al.*, 2004; Bacour *et al.*, 2006). Although the FPAR is the fraction of PAR in the visible band, this intrinsic relationship between FPAR and visible was not linear. Comparatively, the VIs are linear or nearly linear computed directly with two bands reflectance. Therefore, the NN could obtain better R^2 than those vegetation indices from the combination of NIR and visible bands.

In general, LAI makes mostly significant influence on the canopy FPAR, but the effects from some other factors of leaf components on the canopy FPAR can not be neglected, such as soil background, leaf chlorophyll, leaf and soil water content (Myneni and Williams, 1994; Huemmrich and Goward, 1997; Daniel *et al.*, 2006). A few researchers also have studied the leaf chlorophyll content effect on the forest or grass FPAR (Xiao *et al.*, 2005; Gao *et al.*, 2006). Comparatively, for the corn crop, few studies have considered the leaf components effect on the crop canopy FPAR (Daniel *et al.*, 2006). Based on the hyperspectral remote sensing, this study analyzed the hyper-spectra performance on corn FPAR estimation using two methods of VIs and NN, which both revealed that the SWIR has great potential on improving the corn FPAR estimation accuracy.

As we all known, the SWIR were mainly controlled

Table 4 Comparison of different methods for FPAR estimation performances

R^2	Percent (%)						
	VI						NN
	NDVI	SR	RDVI	SAVI	TSAVI	PVI	
0.82–0.84	11.324	15.197	14.080	13.342	8.336	3.004	6.540
0.84–0.86	21.316	13.251	13.721	9.907	10.962	0.091	10.960
0.86–0.88	20.839	7.889	2.527	1.972	1.522	0	21.414
0.88–0.90	1.770	0.065	0	0	0	0	38.047
0.90–0.92	0	0	0	0	0	0	8.986
0.92–0.94	0	0	0	0	0	0	0.607
Maximum	0.8849	0.8852	0.8719	0.8724	0.8688	0.8522	0.9417

by the factor of water, which is also one of the most important elements of vegetation photosynthesis. In this study, the reflectance of the spectral bands being centered at 450 nm, 700 nm, 1450 nm and 1950 nm were also highly correlated with the corn FPAR. These findings were also supported by previous studies (Carter, 1991; Zarco-Tejada *et al.*, 2003), which indicated that the functions in these bands are greatly controlled by chlorophyll or leaf water. However, the soil water content is the main source to leaf water content, and the leaf and the soil water content effects on the canopy were not quantitative assessed for the shortage of abundant data. This will be further investigated in the future based on the water content controlling experiment. But the studied results in this investigation can be used as a reference for choosing remote sensing images and sensor channels in estimating non-point corn canopy FPAR.

5 Conclusions

Based on ground-measured corn hyperspectral reflectance in Jilin Province, Northeast China, the correlation between corn FPAR and hyperspectral reflectance was analyzed. Using different two-band combinations, six VIs and the NN were used for estimating FPAR performance.

The corn canopy FPAR varies little in a single day and retains a nearly constant value, with the exception of slight fluctuations from 10:30 AM to 13:00 PM. The visible and SWIR bands exhibit marked negative correlations with the corn FPAR, which are stronger than the positive correlations between the NIR band and corn FPAR.

Hyperspectral data are very useful in improving FPAR estimation accuracy. Among all the methods, the NN shows the best FPAR estimation performance. The NDVI and SR are better than other VIs for corn FPAR estimation. For all of the VIs, the two-band combinations that achieve the best FPAR estimation performances are from the SWIR and NIR bands; for the NN, however, the best combination is from the NIR and visible bands.

The results of this study could provide references for FPAR estimation and band selection using hyperspectral data. However, in terms of the absence of hyperspectral remote sensing images, corn FPAR estimation from hyperspectral images were not conducted in this study. Therefore, this gap should be addressed in the future investigation.

References

Bacour C, Baret F, Beal D *et al*., 2006. Neural network estimation of LAI, fAPAR, fCover and LAI Cab, from top of canopy MERIS reflectance data: Principles and validation. *Remote Sensing of Environmen*t, 105(4): 313–325. doi: 10.1016/j.rse.2006.07.014

Baret F, Guyot G, Major D, 1989. TSAVI—A vegetation index which minimizes soil brightness effects on LAI and APAR estimation. IEEE *Geoscience and Remote Sensing Symposium*, 3: 1355–1358. doi: 10.1109/IGARSS.1989.576128

Carter G, 1991. Primary and secondary effects of water content on the spectral reflectance of leaves. *American Journal of Botany*, 78(7): 916–924.

Chen J, Cihlar J, 1996. Retrieving leaf area index of boreal conifer forests using Landsat TM images. *Remote Sensing of Environment*, 55(2): 153–162. doi:10.1016/0034-4257(95)00195-6

Curran P, 1989. Remote sensing of foliar chemistry. *Remote Sensing of Environment*, 30(3): 271–278. doi: 10.1016/0034-4257(89)90069-2

Daniel C, Scott J, Edward J, 2006. Validation of MODIS FPAR products in Boreal forests of Alaska. *IEEE Transactions on Geoscience and Remote Sensing*, 44(7): 1818–1828. doi: 10.1109/TGRS.2005.862266

Daughtry C, Gallo K, Goward S *et al.*, 1992. Spectral estimates of absorbed radiation and phytomass production in corn and soybean canopies. *Remote Sensing of Environment*, 39(2): 141–152. doi:10.1016/0034-4257(92)90132-4

Epiphanio J C, 1995. Dependence of NDVI and SAVI on sun/sensor geometry and its effect on fAPAR relationships in alfalfa. *Remote Sensing of Environment*, 51(3): 351–360. doi: 10.1016/0034-4257(94)00110-9

FAO, 2007. Development of Standards for Essential Climate Variables: Fraction of Absorbed Photosynthetically Active Radiation (FAPAR). Available at: www.fao.org/gtos/doc/ECVs/T10/ECV-T10-fAPAR-report-v02.doc.

Fang H L, Liang S L, Senior Member I, 2003. Retrieving keaf area index with a neural network method: Simulation and validation. *IEEE Trancsactions on Geoscience and Remote Sensing*, 41(9): 2502–2602. doi: 10.1109/TGRS.2003.813493

Gallo K, Daughtry C, 1986. Techniques for measuring intercepted and absorbed photosynthetically active radiation in corn canopies. *Agronomy journal*, 78(4): 752–756.

Gao Yanhua, Chen Liangfu, Liu Qinhuo *et al.*, 2006. Research on remote sensing model for FPAR absorbed by chlorophyll. *Journal of Remote Sensing*, 10(5): 798–803. (in Chinese)

Gong P, Pu R, Biging G *et al.*, 2003. Estimation of forest leaf area index using vegetation indices derived from Hyperion hypers-

pectral data. *IEEE Transactions on Geoscience and Remote Sensing*, 41(6): 1355–1362. doi: 10.1109/TGRS.2003.812910

Goward S N, Huemmrich K F, 1992. Vegetation canopy PAR absorptance and the normalized difference vegetation index: An assessment using the SAIL model. *Remote Sensing of Environment*, 39(2): 119–140. doi:10.1016/0034-4257(92)90131-3

Huemmrich K F, Goward S N, 1997. Vegetation canopy PAR absorptance and NDVI: An assessment for ten tree species with the SAIL model. *Remote Sensing of Environment*, 61(2): 254–269. doi: 10.1016/S0034-4257(97)00042-4

Huete A, 1988. A soil-adjusted vegetation index (SAVI). *Remote Sensing of Environment*, 25(3): 295–309. doi: 10.1016/0034-4257(88)90106-X

Jordan C, 1969. Derivation of leaf-area index from quality of light on the forest floor. *Ecology*, 50(4): 663–666.

Knyazikhin Y, Martonchik J, Diner D *et al*., 1998a. Estimation of vegetation canopy leaf area index and fraction of absorbed photosynthetically active radiation from atmosphere-corrected MISR data. *Journal of Geophysical Research*, 103(D24): 32239–32256.

Knyazikhin Y, Martonchik J, Myneni R *et al*., 1998b. Synergistic algorithm for estimating vegetation canopy leaf area index and fraction of absorbed photosynthetically active radiation from MODIS and MISR data. *Journal of Geophysical Research*, 103(D24): 32257–32276.

Kimes D, Nelson R, Manry M *et al.*, 1998. Review article: Attributes of neural networks for extracting continuous vegetation variables from optical and radar measurements. *International Journal of Remote Sensing*, 19(14): 2639–2663.

Krasnopolsky V, Chevallier F, 2003. Some neural network applications in environmental sciences. Part II: Advancing computational efficiency of environmental numerical models. *Neural Networks*, 16(3–4): 335–348. doi: 10.1016/S0893-6080(03)00026-1

Lee Z, Carder K, Mobley C *et al.*, 1999. Hyperspectral remote sensing for shallow waters. 2. Deriving bottom depths and water properties by optimization. *Applied Optics*, 38(18): 3831–3843. doi: 10.1364/AO.38.003831

Lobell D, Asner G, Ortiz-Monasterio J *et al*., 2003. Remote sensing of regional crop production in the Yaqui Valley, Mexico: Estimates and uncertainties. *Agriculture, Ecosystems & Environment*, 94(2): 205–220. doi:10.1016/S0167-8809(02)00021-X

Lyon J G, Yuan D, Lunetta R S *et al.*, 1998. A change detection experiment using vegetation indices. *Photogrammetric Engineering and Remote Sensing*, 64(2): 143–150.

McCallum I, Wagner W, Schmullius C *et al.*, 2010. Comparison of four global FAPAR datasets over northern Eurasia for the year 2000. *Remote Sensing of Environment*, 114(5): 941–949. doi: 10.1016/j.rse.2009.12.009.

Melgani F, Bruzzone L, 2004. Classification of hyperspectral remote sensing images with support vector machines. *IEEE Transactions on Geoscience and Remote Sensing*, 42(8): 1778–1790. doi: 10.1109/TGRS.2004.831865.

Myneni R, Hoffman S, Knyazikhin Y *et al.*, 2002. Global products of vegetation leaf area and fraction absorbed PAR from year one of MODIS data. *Remote Sensing of Environment*, 83(1–2): 214–231. doi: 10.1016/S0034-4257(02)00074-3

Myneni R, Williams D, 1994. On the relationship between FAPAR and NDVI. *Remote Sensing of Environment*, 49(3): 200–211.

Pu R, Gong P, 2004. Wavelet transform applied to EO-1 hyperspectral data for forest LAI and crown closure mapping. *Remote Sensing of Environment*, 91(2): 212–224. doi: 10.1016/j.rse.2004.03.006

Ridao E, Conde J R, 1998. Estimating fAPAR from nine vegetation indices for irrigated and nonirrigated faba bean and semileafless pea canopies. *Remote Sensing of Environment*, 66(1): 87–100. doi: 10.1016/S0034-4257(98)00050-9

Roujean J L, Breon F M, 1995. Estimating PAR absorbed by vegetation from bidirectional reflectance measurements. *Remote Sensing of Environment*, 51(3): 375–384. doi: 10.1016/0034-4257(94)00114-3

Rouse J W, Haas R H, Schell J A *et al.*, 1974. Monitoring vegetation systems in the Great Plains with ERTS. *NASA Goddard Space Flight Center 3d ERTS-1 Symposium*, United States, 1(Section A): 309–317.

Sellers P, Dickinson R, Randall D *et al*., 1997. Modeling the exchanges of energy, water, and carbon between continents and the atmosphere. *Science*, 275(5299): 502. doi: 10.1126/science.275.5299.502

Smith J, 1993. LAI inversion using a back-propagation neural network trained with a multiple scattering model. *IEEE Transactions on Geoscience and Remote Sensing*, 31(5): 1102–1106. doi: 10.1109/36.263783

Song Kaishan, 2005. *Study on the Characteristic of Hyperspectral Reflectance, Polarized Reflectance of Corn and Soybean*. Changchun: Northeast Institute of Geography and Agroecology, Chinese Academy of Sciences. (in Chinese)

Tao Xin, Fan Wenjie, Wang Dacheng *et al.*, 2009. Remote sensing retrieval of FAPAR: Model and analysis. *Journal of Remote Sensing*, 24(7): 741–747. (in Chinese)

Tian Q, Tong Q, Pu R *et al.*, 2001. Spectroscopic determination of wheat water status using 1650–1850 nm spectral absorption features. *International Journal of Remote Sensing*, 22(12): 2329–2338.

Turner D, Gower S, Cohen W *et al.*, 2002. Effects of spatial variability in light use efficiency on satellite-based NPP monitoring. *Remote Sensing of Environment*, 80(3): 397–405. doi: 10.1016/S0034-4257(01)00319-4

Walthall C, Dulaney W, Anderson M *et al.*, 2004. A comparison of empirical and neural network approaches for estimating corn and soybean leaf area index from Landsat ETM+ imagery. *Remote Sensing of Environment*, 92(4): 465–474. doi: 10.1016/j.rse.2004.06.003

Widlowski J L, 2010. On the bias of instantaneous FAPAR estimates in open-canopy forests. *Agricultural and Forest Meteorology*, 150(12): 1501–1522. doi: 10.1016/j.agrformet.2010.07.011

Xiao X, Zhang Q, Hollinger D *et al.*, 2005. Modeling gross primary production of an evergreen needleleaf forest using MODIS and climate data. *Ecological Applications*, 15(3): 954–969.

Yang F, Li J, Gan X *et al.*, 2010. Assessing nutritional status of Festuca arundinacea by monitoring photosynthetic pigments from hyperspectral data. *Computers and Electronics in Agriculture*, 70(1): 52–59. doi: 10.1016/j.compag.2009.08.010

Zarco-Tejada P, Rueda C, Ustin S, 2003. Water content estimation in vegetation with MODIS reflectance data and model inversion methods. *Remote Sensing of Environment*, 85(1): 109–124. doi: 10.1016/S0034-4257(02)00197-9

Zhao Yingshi, 2003. *Principles and Methods of Remote Sensing Application*. Beijing: Science Press, 373–382. (in Chinese)